High-Performance Organolead Halide Perovskite-Based Self-Powered Triboelectric Photodetector

Li Su,[†,⊥] Zhen Xuan Zhao,[†,⊥] Hua Yang Li,[†] Jian Yuan,[†] Zhong Lin Wang,[*,†,‡] Guo Zhong Cao,[*,†,§] and Guang Zhu[*,†]

[†]Beijing Institute of Nanoenergy and Nanosystems, Chinese Academy of Sciences, Beijing 100083, China, [‡]Department of Materials and Engineering, Georgia Institute of Technology, Atlanta, Georgia 30332, United States, and [§]Department of Materials and Engineering, University of Washington, Seattle, Washington 98195-2120, United States. [⊥]L.S. and Z.X.Z. contributed equally.

ABSTRACT We report a $MAPbI_3$-based self-powered photodetector (SPPD). It has a dual sensing mechanism that relies on the joint properties of a photoelectric effect and a triboelectric effect of the perovskite material. Both the photoconductivity and the surface triboelectric density of the $MAPbI_3$-based composite thin film are significantly altered upon solar illumination, which results in considerable reduction of the output voltage. The SPPD exhibits excellent responsivity (7.5 V W^{-1}), rapid response time (<80 ms), great repeatability, and broad detection range that extends from UV to visible regions. This work presents a route to designing high-performance self-powered photodetectors from the aspect of materials.

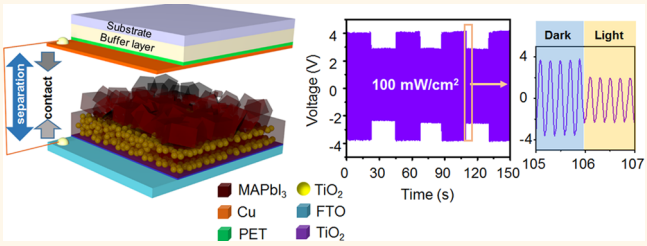

KEYWORDS: organolead halide perovskite · self-powered · triboelectric effect · photodetector

Photodetectors that can convert incident light into an electrical signal are critical for a variety of applications, including optical communications, environmental monitoring, security surveillance, and chemical/biological sensing.[1−4] A great commercialization prospect is expected for photodetectors that have low power consumption, broad-band detection, fast response, and excellent portability. A photodetector normally has a sandwich structure that includes a photosensitive material and two electrodes.[5,6] Recently, organometal trihalide perovskite $MAPbI_3$ has attracted extensive attention due to its low cost,[7] solution-based processing at low temperature,[8] high absorption coefficient of up to 10^{-5} cm^{-1},[9] and extended diffusion length of excitation.[10] By using this material to convert light energy, a great breakthrough in developing high-photovoltage solar cells has been witnessed in recent years.[11,12] Moreover, $MAPbI_3$ has become a promising material for photodetectors due to its excellent light sensitivity and broad-band light absorption.[13] Hu *et al.*[14] reported a broad-band photodetector by using $MAPbI_3$ that is sensitive to a wide spectrum of wavelengths. Dong *et al.*[15] reported another $MAPbI_3$-based photodetector that had excellent photoconductive properties due to the high carrier mobility of the $MAPbI_3$. However, all photodetectors including the recently reported $MAPbI_3$-based ones rely on an external electric power source.

Self-powered sensors represent a new type of sensors that can operate without an electric power source.[16,17] They can generate electric signals on their own by converting other types of energy into electricity that is to be measured. By analyzing the electric signal that is altered by a certain external stimulus, the presence and magnitude of the stimulus can then be derived. Self-powered sensors have been reported for detecting mechanical motions,[18] chemical molecules,[19] thermal agitations,[20] photon excitations,[21] and so on. However, the use of organolead halide perovskite for self-powered photodetection was not reported.

Herein we report a $MAPbI_3$-based self-powered photodetector (SPPD) that utilizes the joint properties of photoelectric effect and triboelectric effect of the perovskite

* Address correspondence to zlwang@binn.cas.cn, gzcao@uw.edu, zhuguang@binn.cas.cn.

Received for review August 11, 2015 and accepted October 15, 2015.

Published online 10.1021/acsnano.5b04995

material. The SPPD exhibits excellent responsivity (7.5 V W^{-1}), rapid response time (<80 ms), great repeatability, and broad detection range that extends from UV to visible regions. By using scanning Kelvin probe microscope (SKPM) and conductive atomic force microscope (CAFM) measurements, we reveal and propose a novel dual sensing mechanism in which both the photoconductivity and the surface triboelectric density of the $MAPbI_3$-based composite thin film are significantly altered upon solar illumination. This work presents a new route to designing high-performance self-powered photodetectors from the aspect of materials.

RESULTS AND DISCUSSION

A SPPD is composed of two separate parts, as illustrated by the device structure shown in Figure 1a. Both are 2 cm × 2 cm in lateral dimensions. The bottom part is constructed on a transparent fluorine-doped tin oxide (FTO) substrate. A compact TiO_2 hole-blocking layer, an electron transport layer of a mesoporous TiO_2 scaffold, and a light-absorption layer of $MAPbI_3$ are fabricated sequentially on the FTO substrate. The upper part is a copper layer deposited on an elastic buffer layer that can enhance the effective contact area between the copper layer and the $MAPbI_3$ layer. The copper layer and the FTO layer act as the upper and the bottom electrodes, respectively, which are connected to the positive and the negative terminals of an electrometer for data acquisition. The detailed fabrication process is presented in the Materials and Methods section. The $MAPbI_3$ has a distorted perovskite structure that crystallizes in the tetragonal *I*4/*mcm* space group at room temperature. It has lead cations in six-fold coordination, surrounded by an octahedron of halide anions together with the organic components $(CH_3NH_3)^+$ in 12-fold cuboctahedral coordination. The significant hybridization between the Pb 6s and the I 5p states is formed in the polyhedron of $[PbI_{6/2}]^-$, as schematically illustrated in Figure 1b. The surface properties of the $MAPbI_3$-based layer are characterized by scanning electronic microscopy (SEM) and atomic force microscopy (AFM). The cross-sectional view in Figure 1c clearly shows the layer-by-layer structure. The mesostructured TiO_2 layer (300 nm thick) on a compact TiO_2 hole-blocking layer (25 nm thick) is filled with crystalline $MAPbI_3$ and covered by a layer of $MAPbI_3$ nanoparticles that are 200 nm in diameter (top-down view in Figure 1d). The AFM measurement results shown in Figure 1e,f reveal an average surface

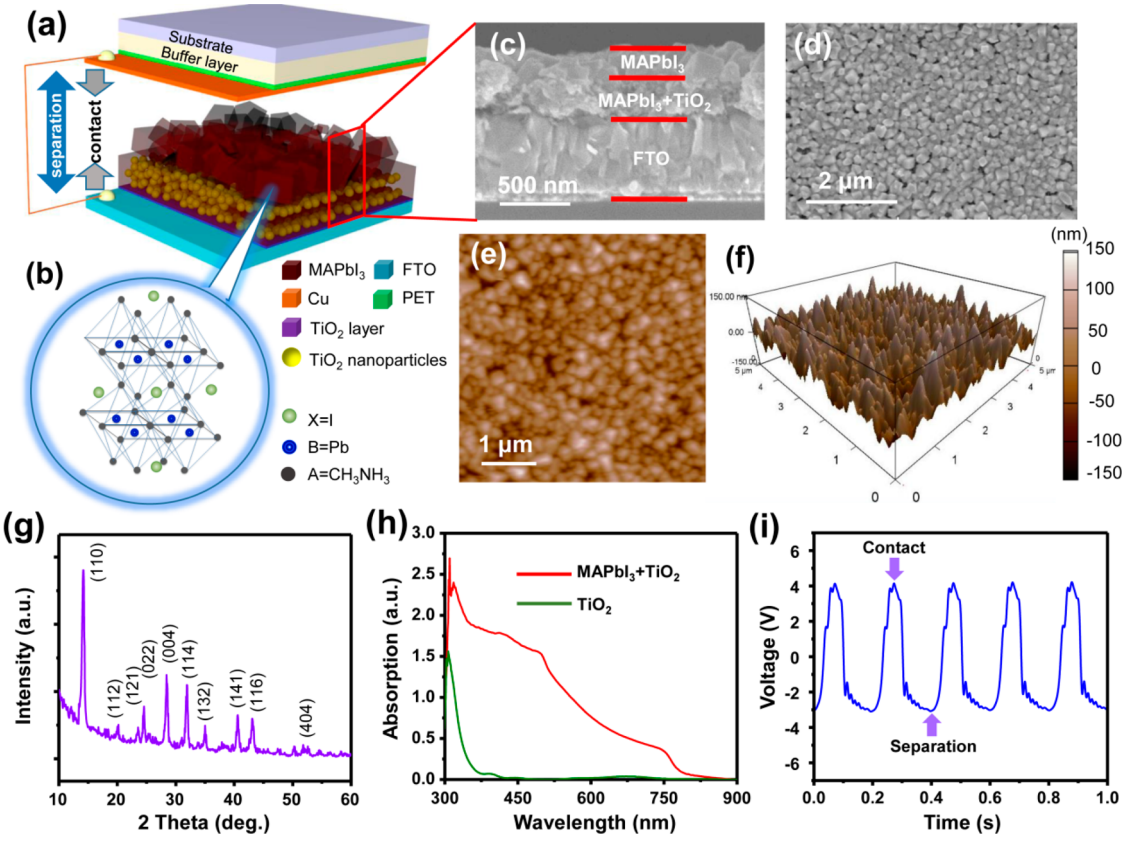

Figure 1. Structure and characterization of a SPPD. (a) Device structure of a SPPD. (b) Three-dimensional schematic representation of the crystal structure of $CH_3NH_3PbI_3$. (c) Cross-sectional and (d) top-down views of the $MAPbI_3$-based film in SEM images. (e) Morphology of the $MAPbI_3$ capping layer measured by AFM and (f) its corresponding three-dimensional graphs. (g) XRD diffraction pattern of the $MAPbI_3$-based film on the FTO glass. (h) UV−vis absorption spectrum of the $MAPbI_3$-based composite film as well as the mesoporous TiO_2 film. (i) Open-circuit voltage (V_{oc}) output of the SPPD without illumination.

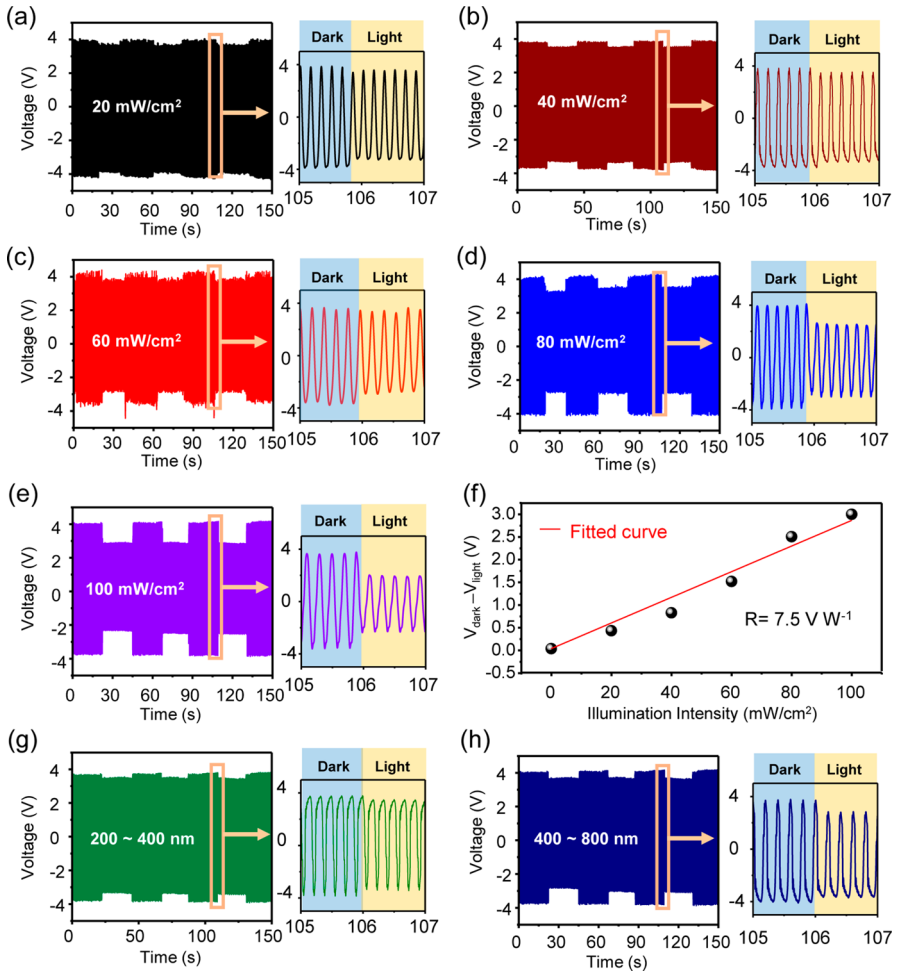

Figure 2. Change of V_{oc} upon repeated illumination that varies in intensity and wavelength, (a) 20 mV/cm^2, (b) 40 mV/cm^2, (c) 60 mV/cm^2, (d) 80 mV/cm^2, (e) 100 mV/cm^2, and their corresponding enlarged views at the moment when the illumination is applied. (f) Light intensity dependence of the voltage change and its linearly fitted curve. The V_{oc} under the illumination of (g) the ultraviolet and (h) the visible portions of the solar spectrum.

roughness of 21 nm. The X-ray diffraction pattern shown in Figure 1g matches well with the tetragonal perovskite structure reported by others.[22] The $MAPbI_3$—TiO_2 composite film has an absorption edge at 760 nm according to the UV—vis absorption spectrum, which is consistent with previous reports.[23] It is noticed that the composite film has high absorption over a broad range, especially in the range of 300—400 nm. This can be ascribable to the high absorption of the mesoporous TiO_2 in the UV region, as shown in Figure 1h.

The SPPD is essentially a triboelectric nanogenerator that can convert mechanical energy into electricity.[24,25] When an external force brings the top copper electrode into repeated contacts with the perovskite layer in a periodic way, triboelectric charges of opposite signs on the contact surfaces induce an oscillating open-circuit voltage (V_{oc}) between the two electrodes, as shown in Figure 1i. The measurable voltage is ascribed to the electric potential difference between the two electrodes.[26] It needs to be noted that the obtained V_{oc} is essentially the voltage that is applied onto the inner resistance of a triboelectric nanogenerator since $MAPbI_3$ as well as TiO_2 is a semiconductor with finite conductivity.

Without illumination, the V_{oc} has a peak-to-peak value of 8 V, as exhibited in Figure 1i. The voltage amplitude is immediately reduced after the SPPD is exposed to the illumination supplied by a solar simulator. Once the illumination is cut off, the voltage amplitude recovers quickly to the original value, as shown in Figure 2a—e. It was found that the variation of the voltage amplitude upon illumination increases as the applied light intensity increases from 20 to 100 mW cm^{-2} at an increment of 20 mW cm^{-2} (Figure 2f). In 1 sun condition, the voltage is reduced by 37.5% to 5 V upon solar illumination. The light intensity dependence of the V_{oc} enables the SPPD to be a viable approach for photodetection.

The responsivity (R) can be defined by the following equation:[27]

$$R = \frac{\Delta V}{A \Delta P} \quad (1)$$

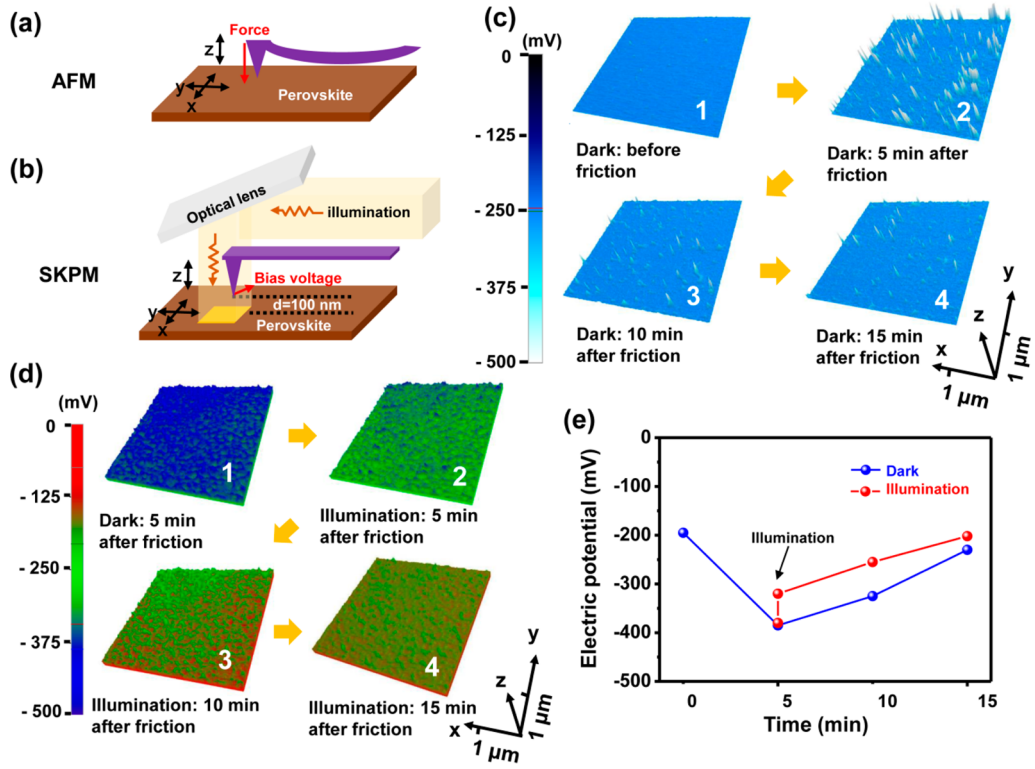

Figure 3. Characterization of surface potential upon illumination. Schematic illustrations of (a) contact-mode AFM and (b) SKPM mode with applied illumination. 3D mappings of the surface potential after friction (c) without the illumination and (d) with the illumination applied 5 min after the friction. (e) Corresponding values of the surface potential as time passes by.

where ΔV is the variation of the voltage amplitude resulting from the increment of light intensity, A is the illuminated area, and ΔP is the light intensity. The change of the voltage amplitude at different light intensities ($V_{dark} - V_{light}$) is plotted in Figure 2f, and the average responsivity can be obtained by linear fitting, which generates a value of 7.5 V W^{-1}. It represents 2−18-fold enhancement over recently reported photodetectors based on $MAPbI_3$.[14,28,29]

Since the electric signal generated by the SPPD is constantly changing, it would be difficult to extract an exact value of the response time. However, it can still be reasonably estimated. As shown in the inset of Figure 2d, the voltage amplitude has a sharp step instead of a gradual changing process, indiciating immediate response to the illumination. The variation completely finishes within one-half of a cycle of the oscillating voltage that equals 80 ms. Therefore, the response time of the SPPD is less than 80 ms, which is superior to many other reported perovskite-based photodetectors.[6,30−32]

Broad-band detection ability is another important merit for a photodetector. Here, specific spectral detection is investigated by using two optical filters that can divide the incident solar illumination into ultraviolet (200−400 nm) and visible regions (400−1000 nm). In both cases, the V_{oc} drops in response to the illumination, although the visible light (Figure 2g) induces a more obvious variation of the V_{oc} than the UV light (Figure 2h). This difference can be explained by the fact that the visible portion of the solar spectrum has a higher intensity and a broader range compared to the UV portion.

It was found that the SPPD has a dual sensing mechanism. The sudden reduction of the V_{oc} upon illumination might be attributed to the change of both surface and bulk properties of the perovskite material. We adopted AFM and SKPM to characterize the surface property of the $MAPbI_3$ upon illumination. First, the $MAPbI_3$ surface was rubbed by an Ir-based tip with Pt coating in the contact mode of AFM, as illustrated in Figure 3a. Then SKPM was employed to monitor the surface potential of the rubbed area at a bias voltage of 3 V, during which illumination is shed onto the rubbed surface (Figure 3b). The obtained surface potential is a direct indicator of the surface charge density. As shown in Figure 3c, the negative surface potential reveals that negative triboelectric charges are generated on the $MAPbI_3$ surface after it is rubbed by the AFM tip. If no illumination is introduced after the rubbing, the surface potential gradually drops as time passes by, which is illustrated in Figure 3c and quantitatively shown in Figure 3e. This is because the triboelectric charges slowly dissipate into the air in an extended period of time and eventually vanish, which is an intrinsic property of triboelectrification on any material if no subsequent contacts/friction take place.[33,34] In comparison, once the illumination is fed in after 5 min

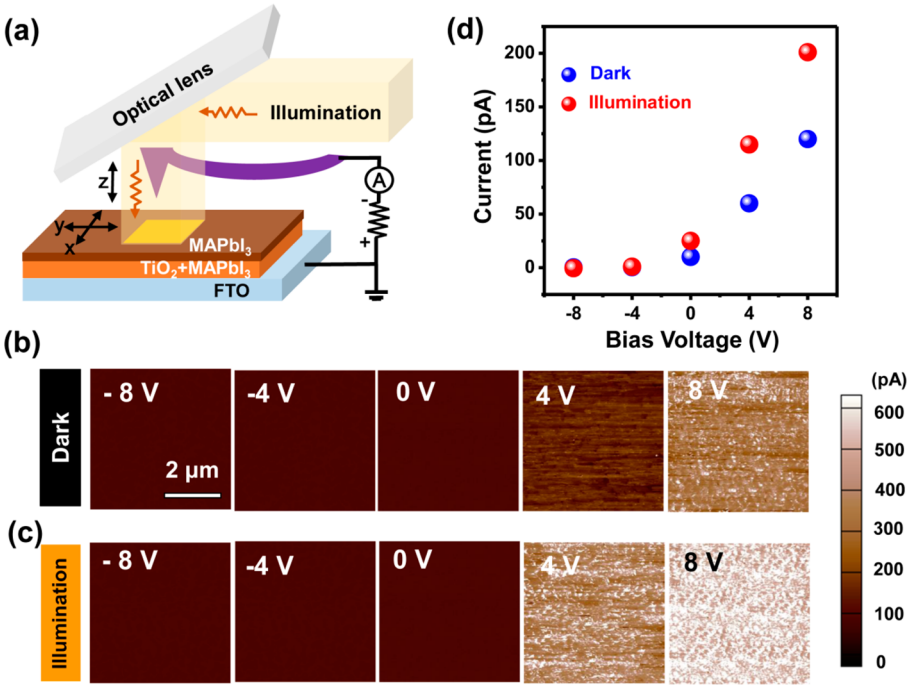

Figure 4. Characterization of the thin-film conductivity upon illumination. (a) Experimental setup of CAFM. The current mapping through the $MAPbI_3$-based composite layer at various bias voltages from −8 to +8 V (b) in darkness and (c) upon illumination at an intensity of 70 mW cm^{-2}. (d) *I*−*V* characteristics through the $MAPbI_3$-based layer.

of the rubbing, the surface potential immediately rises from −385 to −325 mV (Figure 3d,e), indicating that the surface charge density instantaneously decreases as a result of the illumination. Then further reduction of the surface potential is again attributed to the gradual charge dissipation. Therefore, the largely reduced surface triboelectric charge density plays a key role in the sensing mechanism of the SPPD.

The reason for such a quick descent in the surface charge density can be rooted to the light absorption of the perovskite material. Once solar illumination is applied, a large number of electron−hole pairs are generated within the $MAPbI_3$ layer. The electrons are quickly captured by the mesoporous TiO_2 layer that is known for its electron-transporting property. The holes then tend to partially neutralize the negative triboelectric charges on the surface, making the surface charge density plummet as soon as the solar illumination is used.

Moreover, photoconduction of the semiconducting $MAPbI_3$−TiO_2 composite film is another major factor that contributes to the reduced V_{oc} upon solar illumination. Here, CAFM in contact mode was employed. The experimental setup is schemed in Figure 4a, in which current is recorded as the bias voltage varies by using a Pt-coated AFM tip. Solar illumination was directed onto the sample surface *via* an optical lens. The measured current is indicative of the conductivity of the semiconducting composite film between the AFM tip and the FTO substrate. If the bias voltage is negative, very little current that transports through the semiconducting film can be measured regardless of whether the illumination is applied or not, as clearly shown by the current distribution mapping in Figure 4b,c. This results from the one-way transport property of the SPPD owing to the presence of the hole-blocking TiO_2 layer. In contrast, if a positive bias voltage is applied, current can then be measured. As the bias voltage increases, the obtained current rises correspondingly. It was apparently observed that the current through the illuminated sample is significantly higher than the sample in the darkness. This is because the illumination enables a significant enhancement of the conductivity by creating numerous electron−hole pairs. As quantitatively plotted in Figure 4d, the illuminated sample at a bias voltage +8 V has a photocurrent of 200 pA, which is 60% higher than that in the darkness (125 pA). Because of the enhanced conductivity, the inner resistance of the SPPD drops. Therefore, the measured V_{oc} is reduced as soon as the illumination is present.

CONCLUSIONS

In summary, we developed an integrated SPPD based on perovskite material, which demonstrates an excellent performance without reliance on an external power source. It has a rapid response time (<80 ms), a high photoresponsivity (7.5 V W^{-1}), and broad response from UV to visible regions. Based on the CAFM and SKPM measurements, the physical mechanism was interpreted as the immediate alteration of the thin-flim conductivity and the surface charge density

upon illumination. This work demonstrates that the perovskite-based SPPD is a great candidate for applications in light detection and may be extended to applications in other types of self-powered sensors.

MATERIALS AND METHODS

Synthesis and Characterization of Perovskite. The perovskite-based film with the configuration of FTO/compact TiO_2/mesoporous TiO_2 + $CH_3NH_3PbI_3$/$CH_3NH_3PbI_3$ crystalline capping layer was prepared according to the following processes. Typically, FTO glasses were cleaned with detergent, followed by sonication in acetone and ethanol. Then, O_2 plasma cleaner was used to remove organic contaminants for 20 min under 200 Hz. A compact TiO_2 blocking layer was deposited on the cleaned FTO substrate by atomic layer deposition (Picosun SUNALE R-100). $TiCl_4$ and N_2 were used as Ti source and purging gas, respectively. A compact TiO_2 layer with 25 nm thickness was grown on the FTO substrate by 500 cycles at a deposition temperature of 200 °C. TiO_2 paste (Dyesol-18NRT) was diluted by ethanol in a 2:7 weight ratio, spin-coated onto the compact TiO_2 layer at 5500 rpm, and sintered at 500 °C for 30 min to form a mesoporous TiO_2 layer with 300 nm thickness. PbI_2 in DMF solution (462 mg mL^{-1}) was infiltrated into the mesoporous TiO_2 layer by spin-coating at 6500 rpm and drying at 70 °C. After being dried, it was dipped in a CH_3NH_3I solution (9 mg mL^{-1} in 2-propanol) for 30 s and sintered at 70 °C for 30 min. The crystal size of the $CH_3NH_3PbI_3$ capping layer can be controlled by changing the concentration of the CH_3NH_3I in the solution.

The surface morphology, cross section, and crystal structure of the as-fabricated perovskite-based composite film were characterized by scanning electron microscopy (Shimadzu, 2020), atom force microscopy (MFP-3D SPM), and X-ray diffraction (X pert 3), respectively. A UV−vis−NIR spectrophotometer (Shimadzu, UV-3600) was used to analyze the light absorption of the perovskite-based film.

Fabrication of the SPPD. The self-powered photodetector was composed of two parts. On one side, an acrylic substrate with dimensions of 2 cm × 2 cm × 0.2 cm was prepared by laser cutting. A copper layer of 200 nm thickness was deposited by magnetron sputtering as the top triboelectrification layer. On the other side, the mesoporous TiO_2 and $MAPbI_3$ were prepared on a FTO glass, which had lateral dimensions of 2.5 cm × 2.5 cm. Subsequently, two pieces of polyimide films with dimensions of 2.5 cm × 2.5 cm × 0.125 cm were prepared and attached to the substrates at opposite edges. They served as braces that created a gap between the two contact surfaces. Finally, a conducting wire was connected to each of the electrodes for measurement.

Measurements. Open-circuit voltage was measured by Keithley 6517A electrometer under a simulated solar spectrum (AM 1.5, ~100 mW cm^{-2}). The CAFM and SKPM measurements were conducted in a MFP-3D AFM from Park Systems NX-10 in an ambient environment. The Ir-based probe with Pt coating was purchased from Nanoworld (product no. EFM-10).

Conflict of Interest: The authors declare no competing financial interest.

Acknowledgment. This research was supported by the Chinese "thousands talents" program for pioneer researchers. Patents have been filed based on the research presented here.

REFERENCES AND NOTES

1. Zhai, T. Y.; Fang, X. S.; Liao, M. Y.; Xu, X. J.; Li, L.; Liu, B. D.; Koide, Y.; Ma, Y.; Yao, J. N.; Bando, Y.; et al. Fabrication of High-Quality In_2Se_3 Nanowire Arrays toward High-Performance Visible-Light Photodetectors. *ACS Nano* **2010**, *4*, 1596–1602.
2. Law, M.; Kind, H.; Messer, B.; Kim, F.; Yang, P. D. Photochemical Sensing of NO_2 with SnO_2 Nanoribbon Nanosensors at Room Temperature. *Angew. Chem., Int. Ed.* **2002**, *41*, 2405–2408.
3. Jie, J. S.; Zhang, W. J.; Jiang, Y.; Meng, X. M.; Li, Y. Q.; Lee, S. T. Photoconductive Characteristics of Single-Crystal CdS Nanoribbons. *Nano Lett.* **2006**, *6*, 1887–1892.
4. Yang, T. B.; Sun, K.; Liu, X. L.; Wei, W.; Yu, T. Z.; Gong, X.; Wang, D. L.; Cao, Y. Zinc Oxide Nanowire as an Electron-Extraction Layer for Broadband Polymer Photodetectors with an Inverted Device Structure. *J. Phys. Chem. C* **2012**, *116*, 13650–13653.
5. Leung, Y. H.; He, Z. B.; Luo, L. B.; Tsang, C. H. A.; Wong, N. B.; Zhang, W. J.; Lee, S. T. ZnO Nanowires Array P-N Homojunction and Its Application as a Visible-Blind Ultraviolet Photodetector. *Appl. Phys. Lett.* **2010**, *96*, 053102.
6. Xia, H. R.; Li, J.; Sun, W. T.; Peng, L. M. Organohalide Lead Perovskite Based Photodetectors with Much Enhanced Performance. *Chem. Commun.* **2014**, *50*, 13695–13697.
7. Kumar, C. V.; Sfyri, G.; Raptis, D.; Stathatos, E.; Lianos, P. Perovskite Solar Cell with Low Cost Cu-phthalocyanine as Hole Transporting Material. *RSC Adv.* **2015**, *5*, 3786–3791.
8. Dou, L. T.; Yang, Y.; You, J.; Hong, Z.; Chang, W.-H.; Li, G; Yang, Y. Solution-Processed Hybrid Perovskite Photodetectors with High Detectivity. *Nat. Commun.* **2014**, *5*, 5404.
9. Lee, M. M.; Teuscher, J.; Miyasaka, T.; Murakami, T. N.; Snaith, H. J. Efficient Hybrid Solar Cells Based on Meso-Superstructured Organometal Halide Perovskites. *Science* **2012**, *338*, 643.
10. Stranks, S. D.; Eperon, G. E.; Grancini, G.; Menelaou, C.; Alcocer, M. J. P.; Leijtens, T.; Herz, L. M.; Petrozza, A.; Snaith, H. J. Electron-Hole Diffusion Lengths Exceeding 1 Micrometer in an Organometal Trihalide Perovskite Absorber. *Science* **2013**, *342*, 341–344.
11. Bi, C.; Yuan, Y. B.; Fang, Y. J.; Huang, J. S. Low-Temperature Fabrication of Efficient Wide-Bandgap Organolead Trihalide Perovskite Solar Cells. *Adv. Energy Mater.* **2015**, *5*, 1401616.
12. Deng, Y. H.; Peng, E.; Shao, Y. C.; Xiao, Z. G.; Dong, Q. F.; Huang, J. S. Scalable Fabrication of Efficient Organolead Trihalide Perovskite Solar Cells with Doctor-Bladed Active Layers. *Energy Environ. Sci.* **2015**, *8*, 1544–1550.
13. Zhu, X.; Su, H. B.; Marcus, R. A.; Michel-Beyerle, M. E. Computed and Experimental Absorption Spectra of the Perovskite $CH_3NH_3PbI_3$. *J. Phys. Chem. Lett.* **2014**, *5*, 3061–3065.
14. Hu, X.; Zhang, X. D.; Liang, L.; Bao, J.; Li, S.; Yang, W. L.; Xie, Y. High-performance Flexible Broadband Photodetector Based on Organolead Halide Perovskite. *Adv. Funct. Mater.* **2014**, *24*, 7373–7380.
15. Dong, R.; Fang, Y. J.; Chae, J.; Dai, J.; Xiao, Z. G.; Yuan, Y. B.; Centrone, A.; Zeng, X. C.; Huang, J. S. High-Gain and Low-Driving-Voltage Photodetectors Based on Organolead Triiodide Perovskites. *Adv. Mater.* **2015**, *27*, 1912–1918.
16. Meng, B.; Tang, W.; Too, Z. H.; Zhang, X. S.; Han, M. D.; Liu, W.; Zhang, H. X. A Transparent Single-Friction-Surface Triboelectric Generator and Self-Powered Touch Sensor. *Energy Environ. Sci.* **2013**, *6*, 3235–3240.
17. Hu, Y. F.; Xu, C.; Zhang, Y.; Lin, L.; Snyder, R. L.; Wang, Z. L. A Nanogenerator for Energy Harvesting from a Rotating Tire and its Application as a Self-Powered Pressure/Speed Sensor. *Adv. Mater.* **2011**, *23*, 4068–4071.
18. Lin, L.; Wang, S.; Niu, S.; Liu, C.; Xie, Y.; Wang, Z. L. Noncontact Free-Rotating Disk Triboelectric Nanogenerator as a Sustainable Energy Harvester and Self-Powered Mechanical Sensor. *ACS Appl. Mater. Interfaces* **2014**, *6*, 3031–3038.
19. Yu, B. W.; Fu, Y. M.; Wang, P. L.; Zhao, Y. Y.; Xing, L. L.; Xue, X. Y. Enhanced Piezo-Humidity Sensing of a Cd−ZnO Nanowire Nanogenerator as a Self-Powered Active Gas Sensor by Coupling the Piezoelectric Screening Effect and

Dopant Displacement Mechanism. *Phys. Chem. Chem. Phys.* **2015**, *17*, 10856–10860.
20. Yang, Y.; Wang, S. L.; Zhang, Y.; Wang, Z. L. Pyroelectric Nanogenerators for Driving Wireless Sensor. *Nano Lett.* **2012**, *12*, 6408–6413.
21. Lin, Z. H.; Cheng, G.; Yang, Y.; Zhou, Y. S.; Lee, S. M.; Wang, Z. L. Triboelectric Nanogenerator as an Active UV photodetector. *Adv. Funct. Mater.* **2014**, *24*, 2810–2816.
22. Heo, J. H.; Im, S. H.; Noh, J. H.; Mandal, T. N.; Lim, C. S.; Chang, J. A.; Lee, Y. H.; Kim, H. j.; Sarkar, A.; Nazeeruddin, M. K.; et al. Il. Efficient Inorganic−Organic Hybrid Heterojunction Solar Cells Containing Perovskite Compound and Polymeric Hole Conductors. *Nat. Photonics* **2013**, *7*, 486–491.
23. Bi, C.; Shao, Y. C.; Yuan, Y. B.; Xiao, Z. G.; Wang, C. G.; Gao, Y. L.; Huang, J. S. Understanding the Formation and Evolution of Interdiffusion Grown Organolead Halide Perovskite Thin Films by Thermal Annealing. *J. Mater. Chem. A* **2014**, *2*, 18508–18514.
24. Hatch, S. M.; Briscoe, J.; Dunn, S. A. Self-Powered ZnO-Nanorod/CuSCN UV Photodetector Exhibiting Rapid Response. *Adv. Mater.* **2013**, *25*, 867–871.
25. Yang, Q.; Liu, Y.; Li, Z. T.; Yang, Z. Y.; Wang, X.; Wang, Z. L. Self-Powered Ultrasensitive Nanowire Photodetector Driven by a Hybridized Microbial Fuel Cell. *Angew. Chem., Int. Ed.* **2012**, *51*, 6443–6446.
26. Wei, X. Y.; Zhu, G.; Wang, Z. L. Surface-Charge Engineering for High-Performance Triboelectric Nanogenerator Based on Identical Electrification Materials. *Nano Energy* **2014**, *10*, 83–89.
27. Rai, S. C.; Wang, K.; Ding, Y.; Marmon, J. K.; Bhatt, M.; Zhang, Y.; Zhou, W. L.; Wang, Z. L. Piezo-Phototronic Effect Enhanced UV/Visible Photodetector Based on Fully Wide Band Gap Type-II ZnO/ZnS Core/Shell Nanowire Array. *ACS Nano* **2015**, *9*, 6419–6427.
28. Li, D.; Dong, G. F.; Li, W. Z.; Wang, L. D. High Performance Organic-Inorganic Perovskite-Optocoupler Based on Low-Voltage and Fast Response Perovskite Compound Photodetector. *Sci. Rep.* **2015**, *5*, 7902.
29. Sutherland, B. R.; Johnston, A. K.; Ip, A. H.; Xu, J. X.; Adinolfi, V.; Kanjanaboos, P.; Sargent, E. H. Sensitive, Fast, and Stable Perovskite Photodetectors Exploiting Interface Engineering. *ACS Photonics* **2015**, *2*, 1117.
30. Zhuo, S. F.; Zhang, J. F.; Shi, Y. M.; Huang, Y.; Zhang, B. Self-Template-Directed Synthesis of Porous Perovskite Nanowires at Room Temperature for High-Performance Visible-Light Photodetectors. *Angew. Chem., Int. Ed.* **2015**, *54*, 5693–5696.
31. Lee, Y. B.; Kwon, J.; Hwang, E.; Ra, C. H.; Yoo, W. J.; Ahn, J. H.; Park, J. H.; Cho, J. H. High-Performance Perovskite-Graphene Hybrid Photodetector. *Adv. Mater.* **2015**, *27*, 41–46.
32. Wang, Y. S.; Zhang, Y. P.; Lu, Y.; Xu, W. D.; Mu, H. R.; Chen, C. Y.; Qiao, H.; Song, J. C.; Li, S. J.; Sun, B. Q.; et al. Hybrid Graphene-Perovskite Phototransistors with Ultrahigh Responsivity and Gain. *Adv. Opt. Mater.* **2015**, DOI: 10.1002/adom.201500150.
33. Baytekin, H. T.; Patashinski, A. Z.; Branicki, M.; Baytekin, B.; Soh, S.; Grzybowski, B. A. The Mosaic of Surface Charge in Contact Electrification. *Science* **2011**, *333*, 308–312.
34. Zhou, Y. S.; Liu, Y.; Zhu, G.; Lin, Z. H.; Pan, C. F.; Jing, Q. S.; Wang, Z. L. *In situ* Quantitative Study of Nanoscale Triboelectrification and Patterning. *Nano Lett.* **2013**, *13*, 2771–2776.